Regular Article

Removal of chromium (VI) from aqueous solutions using surface modified composite nanofibers

Alaa Mohamed [a,b,d,*], W.S. Nasser [f], T.A. Osman [c], M.S. Toprak [a], M. Muhammed [a,e], A. Uheida [a,*]

[a] Department of Materials and Nano Physics, KTH-Royal Institute of Technology, SE 16440 Stockholm, Sweden
[b] Egypt Nanotechnology Center, EGNC, Cairo University, 12613 Giza, Egypt
[c] Mechanical Design and Production Engineering Department, Cairo University, 12613 Giza, Egypt
[d] Production Engineering and Printing Technology Department, Akhbar El Yom Academy, 12655 Giza, Egypt
[e] Alexandria University, 11559 Alexandria, Egypt
[f] Research Institute of Medical Entomology, 12611 Giza, Egypt

GRAPHICAL ABSTRACT
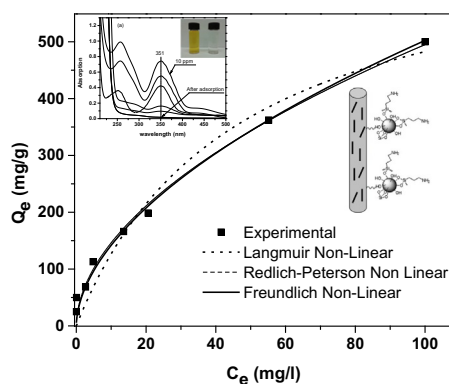
ARTICLE INFO

ABSTRACT

A novel material composite nanofibers (PAN-CNT/TiO$_2$-NH$_2$) based on adsorption of Cr(VI) ions, was applied. Polyacrylonitrile (PAN) and carbon nanotube (CNTs)/titanium dioxide nanoparticles (TiO$_2$) functionalized with amine groups (TiO$_2$-NH$_2$) composite nanofibers have been fabricated by electrospinning. The nanostructures and the formation process mechanism of the obtained PAN-CNT/TiO$_2$-NH$_2$ composite nanofibers are investigated using FTIR, XRD, XPS, SEM, and TEM. The composite nanofibers were used as a novel adsorbent for removing toxic chromium Cr(VI) in aqueous solution. The kinetic study, adsorption isotherm, pH effect, initial concentration, and thermodynamic study were investigated in batch experiments. The composite nanofibers had a positive effect on the absorption of Cr(VI) ions under neutral and acidic conditions, and the saturated adsorption reached the highest when pH was 2. The adsorption equilibrium reached within 30 and 180 min with an initial solution concentration increasing from 10 to 300 mg/L, and the process can be better described using nonlinear pseudo first than nonlinear pseudo second order model and Intra-particle diffusion. Isotherm data fitted well using linear and nonlinear Langmuir, Freundlich, Redlich-Peterson, and Temkin isotherm adsorption model. Thermodynamic study

---

* Corresponding authors at: Department of Materials and Nano Physics, KTH-Royal Institute of Technology, SE 16440 Stockholm, Sweden.
 E-mail address: alakha@kth.se (A. Mohamed).

showed that the adsorption process is exothermic. The adsorption capacity can remain up to 80% after 5 times usage, which show good durability performance. The adsorption mechanism was also studied by UV–vis and XPS.

1. Introduction

Chromium is a natural metal, commonly found in wastewaters, which is originated from several industrial processes such as electroplating industries, military purposes, textile dyeing, paint, leather tanneries, and pigment industries as critical industry materials [1,2]. Chromium possesses two oxidation states Cr(VI) and Cr (III). Cr(VI) is highly toxic, carcinogenic, mutagenic to most of the living organisms when its concentration level is higher than 0.05 ppm, and extremely mobile than Cr(III) [3–5]. Therefore, there is a great importance to remove Cr(VI) from aqueous solution, to prevent the deleterious impact of the Cr(VI) on the human health. Several methods, such as adsorption, reduction, solvent extraction, precipitation, reverse osmosis have been used for removal of Cr(VI) from industrially polluted wastewaters [6–12]. However, most of these techniques have several limitations and drawbacks, and they require high energy or massive use of reducing agents and they are not used widely [5,6]. In particular, adsorption is considered to be simple, economical, and remains one of the most attractive approaches for treating Cr(VI).

Several kinds of materials were used as an adsorbent for the removal of chromium, such as active carbon [13,14], metal oxide nanoparticles [15,16] and biomaterials [17,18]. Among the adsorbents available currently, TiO_2 based adsorbents have been widely used for effective removal of chromium from the polluted water. They have great advantages showing higher removal capacities owing to their outstanding adsorption activities, due to its high adsorption capacities, nontoxic material, inert nature, and highly porous structure [19]. Moreover, the presence of high concentration of hydroxyl groups on the surface of TiO_2 will interact and adsorb pollutant in water [20]. Surface modifications of CNTs have been applied recently to enhance the dispersion property and adsorption capacities of CNTs [21–26]. However, some of these adsorbents have some main drawbacks related to the complexity of the separation process of adsorbent from the solution after the adsorption stage, which will increase the operating cost. In order to avoid this problem, some researchers used nanofibers for the adsorption of several contaminants. PAN-CNT composite system was chosen as the template for loading TiO_2-NH_2 NPs due to that PAN possessed good electrospinnablity, simultaneously, a large number of hydroxyl groups and amine groups existing on the surface of composite nanofiber as well as its non-toxic nature [27,28]. PAN fibers with amine groups were used for the removal of several metal ions [29]. In this regard, nanofibers with nanoparticles were investigated for removal Cr (VI) from aqueous solution [30–34].

In the present work, a novel PAN-CNT/TiO_2-NH_2 composite nanofibers was fabricated for removal of Cr(VI) from aqueous solutions and can be easily separated from the aqueous media. The adsorption kinetics, isotherms and thermodynamic were investigated by fitting the experimental data with different models. The possible adsorption mechanism was provided by testing the adsorption performance under different solution pH values, and initial concentration of the substrate. In addition, the PAN-CNT/TiO_2-NH_2 composite nanofibers were characterized by SEM, TEM, XRD, XPS and FTIR. We anticipated that this composite nanofiber showed promising potential for wastewater treatment.

2. Experimental

2.1. Materials

Multi-walled carbon nanotubes (MWNTs, purity 95 wt.%; diameter: 10–40 nm; length: about 20 μm), CNT synthesis procedure is described elsewhere [35,36]. Potassium dichromate ($K_2Cr_2O_7$), Polyacrylonitrile, PAN (MW = 150,000); hydroxylamine hydrochloride ($NH_2OH·HCl$), sodium carbonate (Na_2CO_3), N,N-dimethylformamide (DMF), sodium hydroxide (NaOH) and hydrochloric acid (HCl), titanium dioxide particulate powder (Degussa P-25), and 3-aminopropyltriethoxysilane (APTES), were purchased from Sigma Aldrich). All chemicals were used as received without any further purification.

2.2. Preparation of electrospun composites nanofibers

10 g DMF solution of PAN (9 wt.%) was mixed for 2 h. In parallel, 3 wt.% of functionalized CNTs were dissolved in DMF for 15 min and sonicated for 30 min. The mixture of PAN and CNTs was magnetically stirred for 30 min and then sonicated for 3 h. The above solution was loaded into a 5 ml syringe, with applied voltage of 25 kV and the tip-to-collector distance was 15 cm. The fabrication of PAN-CNT nanofibers functionalized with amino groups was described elsewhere [27]. 8 g of NH_2OH·HCl and 6 g of Na_2CO_3 was dissolved in 100 ml distilled water and added to the nanofibers. The solution and the prepared PAN-CNT nanofibers were heated to 40 °C for 6 h. After that we remove the remaining salts by washing the nanofibers with distilled water and were dried in air. The surface functionalization of TiO_2 NPs with the amino group was carried out according to a well-established procedure [37]. 10 mL distilled water and 0.5 g of TiO_2 was mixed and the value of pH was adjusted to 11 with sodium hydroxide, to facilitate the adsorption of the hydroxyl group. The hydroxyl group rich TiO_2 NPs were washed twice with 20 mL of methanol to remove the excessive sodium hydroxide, and then dried in a vacuum oven at room temperature for use. Subsequent TiO_2 NPs was dispersed in 100 mL of toluene via Ultrasonication for 30 min. Subsequently, 3 mL of silane was added to the solution. The suspension was further refluxed at 110 °C for 24 h leading to the NH_2 functional group on the titania surface. The reaction product was centrifuged and washed three times with water, followed by methanol to remove the unreacted silane coupling agents, and then dried in a vacuum oven. The crosslinking of the amino functionalized composite nanofibers (PAN-CNT-NH_2) to TiO_2-NH_2 via the amine side was carried out as follow: PAN-CNT-NH_2 composite nanofibers were weighed and immersed in the crosslinking medium containing 2.5 wt.% Glutaraldehyde (GA), and kept shaking for 24 h at room temperature. After the activation reaction of the composite nanofibers was completed, the GA crosslinking medium was removed and then 2 ml of an aqueous dispersion of functionalized TiO_2 was added to the nanofibers for 24 h. The crosslinked composite nanofibers were washed with ethanol followed by distilled water to remove the excess of non-crosslinked nanoparticles and then the composite nanofibers were dried in air at room temperature.

2.3. Characterization

The crystal phase of PAN-CNT/TiO$_2$-NH$_2$ was analyzed by a Bruker D8 Advance X-ray diffraction (XRD) with Cu Ka radiation ($\lambda = 0.15406$ nm) and the accelerating voltage and emission current were 40 kV and 40 mA, respectively. The morphology and microstructure of PAN-CNT/TiO$_2$-NH$_2$ was recorded by scanning electron microscopy (SEM, Gemini Zeiss-Ultra 55), and transmission electron microscope (TEM, JEOL-2100F). Fourier transform infrared (FTIR) spectroscopy were recorded on a Thermo Scientific Nicolet iS10 spectrometer in the range of 600–4000 cm^{-1}. The concentration of Cr(VI) was measured using an Inductively Coupled Plasma Optical Emission Spectroscopy (ICP-OES) (Thermo Fisher iCAP 6500). A ESCALAB 250Xi XPS (Thermo, U.S.) and UV–vis were used in the surface analysis of the resulting PAN-CNT/TiO$_2$-NH$_2$ composite nanofiber adsorbent before and after Cr(VI) adsorption.

2.4. Adsorption of Cr(VI)

The Adsorption of Cr(VI) in aqueous solution was carried out in a 100 mL quartz reactor containing 25 mg composite nanofibers and 50 mL 10 ppm Cr(VI). The pH values of Cr (VI) solution were measured using a pH-meter (WTW pH-330, Germany) and adjusted between 2 and 9 by the addition of HCl or NaOH solutions. Composite nanofibers were dispersed in Cr(VI) solution under shaking condition at room temperature, then 3 mL of the suspension was taken from the reactor at a scheduled interval. Isothermal studies at different temperatures (20 °C, 40 °C, and 60 °C) were carried out by adding the composite nanofibers into 50 ml of Cr(VI) solution of varying concentrations from 10 to 300 ppm at pH 2. The concentration of chromium prior to and after adsorption were measured using UV–vis and ICP. The equilibrium adsorption capacity (q$_e$) was determined using Eq. (1), while % removal of Cr(VI) was calculated using Eq. (2).

$$q_e = \frac{(C_0 - C_e) \times V}{m} \tag{1}$$

$$(\%)\ \text{Removal} = \left(\frac{C_0 - C_e}{C_0}\right) \times 100 \tag{2}$$

where C$_0$ is the initial chromium concentration (mg/L) and C$_e$ is the chromium concentration in the aqueous solution at equilibrium (mg/L), V is the total aqueous volume (L), and m is the mass of the composite nanofibers (g). Thermodynamic parameters such as ΔH^0, ΔS^0, ΔG^0 were also evaluated from equilibrium data.

3. Results and discussions

3.1. Characterization of PAN-CNT/TiO$_2$-NH$_2$ nanofiber

Fig. 1a and b represents SEM images of the PAN and PAN-CNT/TiO$_2$-NH$_2$ nanofiber, showing smooth surface of PAN nanofibers with fiber diameters ranged from approximately 120 nm. For PAN-CNT/TiO$_2$-NH$_2$ nanofiber, the diameters of the PAN nanofibers increased about 90 nm with rough surface compared to the PAN. Fig. 1c represents the TEM image of the prepared PAN-CNT/TiO$_2$-NH$_2$, indicate that the TiO$_2$ are dispersed and immobilized onto the PAN nanofibers and have a relatively dense and uniform distribution.

The crystal phase structure of the PAN-CNT/TiO$_2$-NH$_2$ nanofibers was characterized by XRD measurement as shown in Fig. 2a. The XRD patterns of the PAN-CNT/TiO2-NH2 nanofibers show a very strong anatase peak is observed at 2θ of 25.41°, assigned to (1 0 1) plane. Other anatase peaks are observed at 2θ of 37.96° (0 0 4), and 48.18° (2 0 0). The positions of all diffraction peaks correspond to anatase TiO$_2$ and they coincide well with the reported value [38]. However, a weak rutile peak is observed at 2θ of 54.36°, and 62.92°, assigned to (2 1 1), and (0 0 2) plane. In addition, maximum diffraction peak is observed at 2θ of 17.18° and 28.6° represented the crystallographic planes in PAN, while the other peak at 2θ of 10.98° confirms the existence of a C(0 0 2) peak of CNTs. In addition, the FTIR spectrum of PAN nanofiber Fig. 2b exhibited the absorption peaks of a stretching vibration at 2240 cm^{-1} (C≡N), 1732 cm^{-1} (C=O), and 1455 cm^{-1} (C—O), which
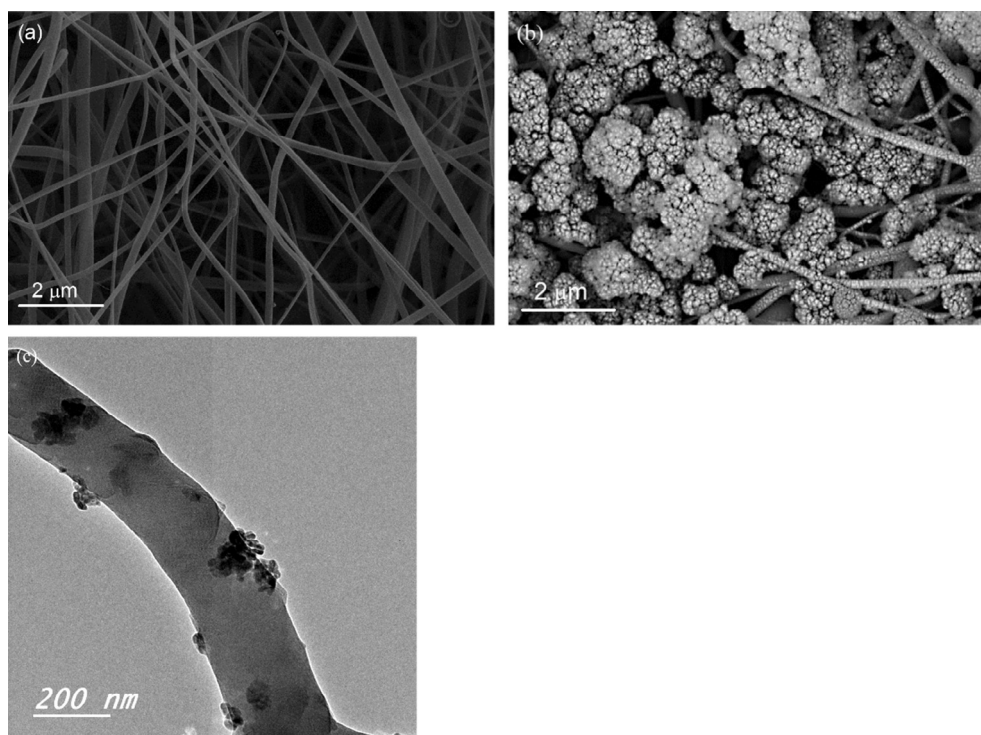

Fig. 1. SEM images of (a) PAN nanofibers, (b) PAN-CNT/TiO$_2$-NH$_2$, and (c) TEM image of PAN-CNT/TiO$_2$-NH$_2$.
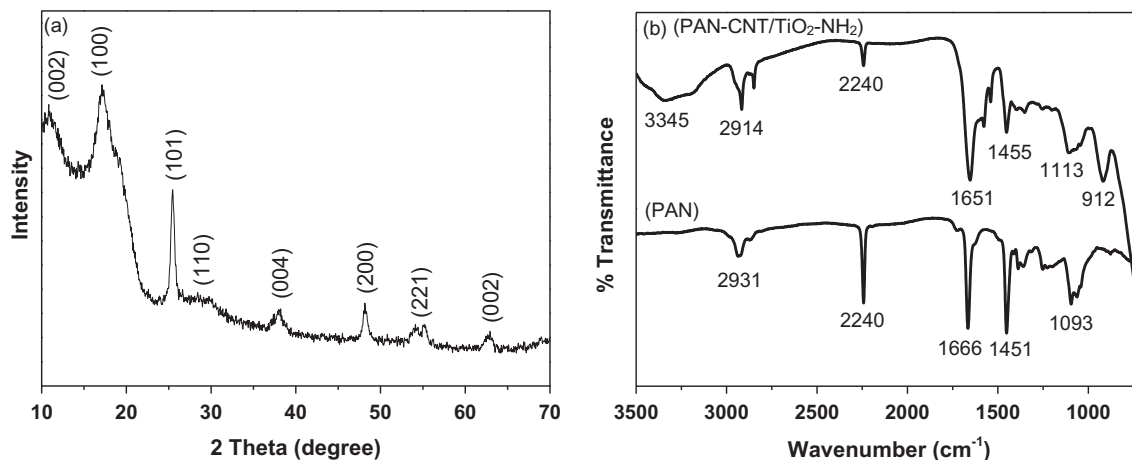
Fig. 2. (a) XRD patterns and (b) FTIR spectrum of the PAN-CNT/TiO$_2$-NH$_2$.

suggests that the PAN was a copolymer of acrylonitrile and methy-lacrylate [29]. Also, the peaks at 1248 cm^{-1} and 1352 cm^{-1} are assigned to the aliphatic —CH— group vibrations of different modes in CH and CH$_2$, respectively. The FTIR spectrum of PAN-CNT/TiO$_2$-NH$_2$ nanofiber shows the absorption peak at 3170–3500 cm^{-1} and 1668 cm^{-1} corresponding to stretching vibrations of the —OH. It can be observed that there are broad peaks at 3345 and 1638 cm^{-1}, which correspond to the surface adsorbed water and hydroxyl groups. The transmittance peak at 1620 and 1452 cm^{-1} were assigned to the (NH$_2$) group and the absorption bands at 1451, 1093, and 912 cm^{-1} were assigned to the C—H, C—C, and N—O, respectively [28]. The peak centered at ~1002 cm^{-1} due to characteristic O—O stretching vibration. The sharp peak at 1455 cm^{-1} can be attributed to the lattice vibrations of TiO$_2$. The absorption band at 1651 cm^{-1} was caused by a bending vibration of coordinated H$_2$O as well as Ti—OH.

3.2. Effect of pH value on the adsorption performance

The pH value of the solution had significant influence on the adsorption of Cr(VI) for the composite nanofibers [32,39]. The influence of the pH value on the adsorption of Cr(VI) was studied in the range of 2–9 as shown in Fig. 3. The composite nanofibers exhibit much higher adsorption capacity under strong acidic condi-

tion rather than in neutral and alkaline conditions. This may be attributed that, the predominate ionic species of Cr(VI) was hydrogen chromate (HCrO$_{4-}$) and dichromate (Cr$_2$O$_7^{2-}$) are negatively charged while the TiO$_2$ is positively charged with the species TiOH$_2^+$ under the pH value from 2 to 5 [40]. Thus, electrostatic attraction between anionic chromate species and the positively charged surface can lead to a strong adsorption of Cr(VI) at low pH [19]. On the other hand, when the pH was above 5, the amount of CrO$_4^{2-}$ increased, while the TiO$_2$ surface becomes gradually more negatively charged with the species TiO$^-$ which was hard to be adsorbed by the adsorbent. In addition, the electrostatic repulsion between the negatively charged surface and chromate species leads to inhibited adsorption of Cr(VI) [41]. On the other hand, the acidic medium facilitates the adsorption capacity of Cr(VI) because of the existence of abundant H$^+$ that adsorbed onto the surface of TiO$_2$, which have a large surface proton exchange capacity. The photogenerated electrons can be captured by the adsorbed H$^+$ to form H$_{ads}$, which is able to adsorbed Cr(VI).

3.3. Adsorption kinetics

Adsorption kinetics are one of the most important parameters for describing the adsorption efficiency. Kinetics adsorption is performed to evaluate the equilibrium time at the different concentra-
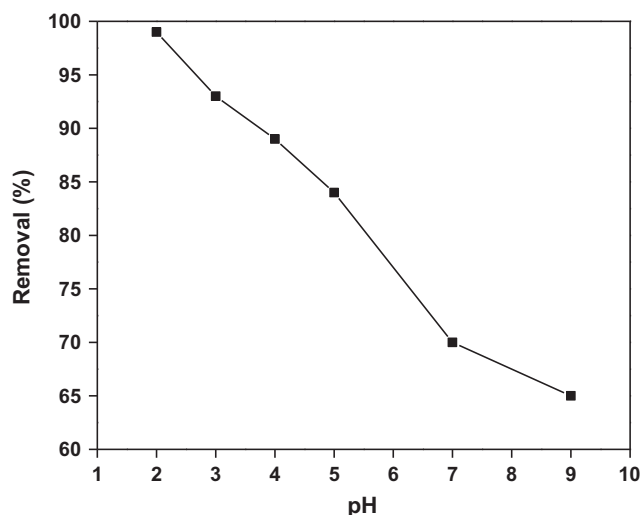

Fig. 3. Effect of pH on the removal of Cr(VI) for the PAN-CNT/TiO$_2$-NH$_2$ composite nanofibers.
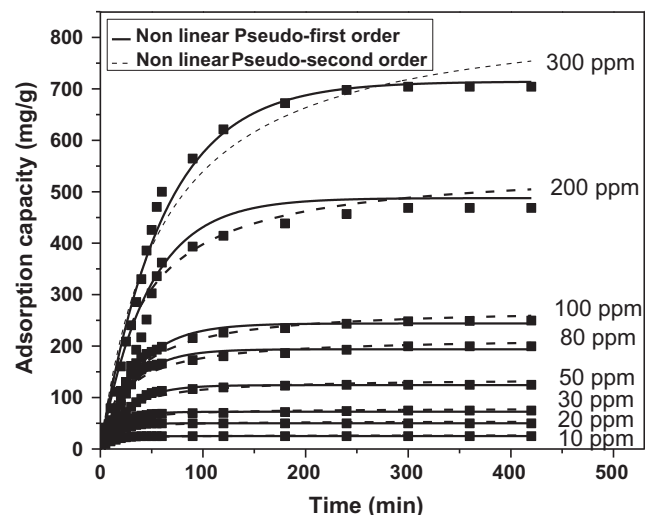

Fig. 4. Nonlinear first-order and second-order plot for the adsorption of Cr(VI) using composite nanofibers.

tion on the adsorption capacity of Cr(VI) as shown in Fig. 4. It demonstrated that the Cr(VI) adsorption capacity of PAN-CNT/TiO$_2$-NH$_2$ increases gradually with increasing the concentrations until an equilibrium was established. The removal of Cr(VI) occurred rapidly and reached adsorption equilibrium within 30 min for 10 ppm, while for 300 ppm take 3 h to reach adsorption equilibrium, and after that the adsorption of Cr(VI) becomes stagnant. It is further observed that the maximum adsorption capacity of Cr(VI) is 704 mg/g. This phenomenon may be due to the electrostatic interaction between the positive protonated amidine, amine groups and negative Cr(VI) ions beside the high density of active sites of PAN-CNT/TiO$_2$-NH$_2$ nanofiber [42]. Therefore, the adsorption process was very fast at short adsorption equilibrium time. Two kinetic models, nonlinear pseudo-first-order Eq. (3), and nonlinear pseudo-second-order Eq. (4), are utilized to fit the experimental data and evaluate the adsorption kinetic process [43–46].

$$q_t = q_e(1 - e^{-k_1 t}) \tag{3}$$

$$q_t = \frac{k_2 q_e^2 t}{1 + k_2 q_e t} \tag{4}$$

where q$_e$ and q$_t$ are the adsorption capacities of Cr(VI) (mg/g) at equilibrium time and at any instant of time t (min), respectively. Where k$_1$ is the rate constant of nonlinear pseudo-first order adsorption (1/min), and k$_2$ is the rate constant of nonlinear pseudo-second order (g/mg min). The correlation coefficient (R^2) for the nonlinear pseudo first order kinetics model is higher than that for the pseudo second order kinetics model indicated that the adsorption kinetics closely followed the nonlinear pseudo first order model as shown in Fig. 4 and Table 1.

Furthermore, the intra-particle diffusion model is used to acquire information needed to assess the suitability, effectiveness of the adsorption process and identify the possible rate controlling step. The intra-particle diffusion model can be described by Eq. (5) [47]:

$$q_t = K_{id} t^{\frac{1}{2}} + C \tag{5}$$

where C is the intercept related to the thickness of the boundary layer and K_{id} is the rate constant of intra-particle diffusion (mg/g/min$^{1/2}$), which can be fitted with the experimental data presented in the plot of q_t versus $t^{1/2}$ depicted in Fig. 5. As can be seen from Fig. 5 and Table 2, the adsorption plot of Cr(VI) pass through the origin concluded that intra-particle diffusion was rate the controlling step [48]. The high value of K$_{id}$ increases from 4.54 to 53.46 mg/g/min$^{1/2}$ with an increase in initial concentrations from 10 to 300 mg/L indicates that composite nanofibers exhibit fast removal rate of Cr(VI) from aqueous solutions [49]. In similar studies for the evaluation of k$_{id}$ values in the same concentration range, Madhumita et al. obtained 5.33 –11.36 mg/g/min$^{1/2}$ using PPy-PANI nanofibers [50], Talreja et al. using Fe-PhB-A-CNF achieved 3.88 mg/g/min$^{1/2}$ [31].
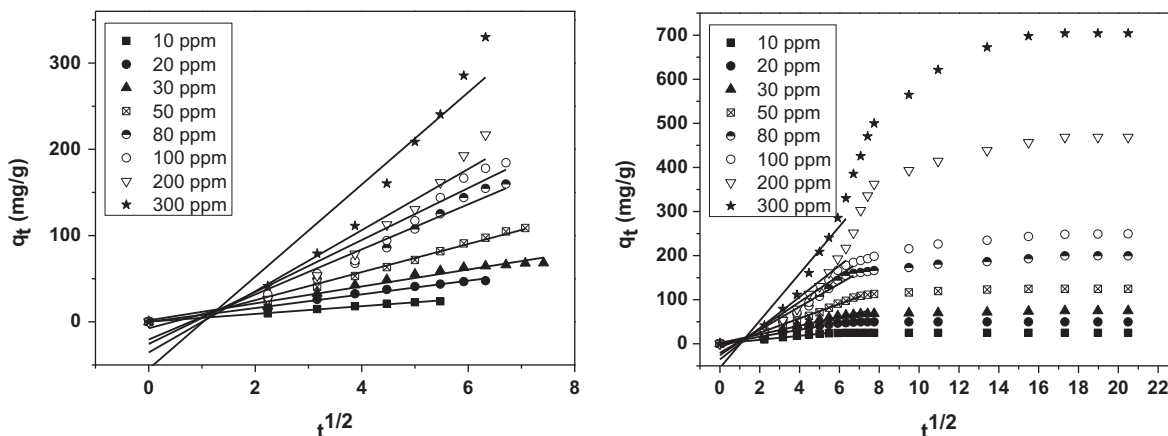
3.4. Adsorption isotherm

Adsorption isotherms were investigated to exhibit the adsorption capacity of the composite nanofibers for the Cr(VI) removal. The effect of temperature on adsorption of Cr(VI) has been investigated at 20, 40 and 60 °C. The linear and nonlinear Langmuir, Freundlich, and Redlich-Peterson isotherms models are conventional models that were used to fit the experimental data [51–54]. The Langmuir model assumes that the adsorption of Cr(VI) occurs as a monolayer on a homogeneous adsorption surface and is expressed by the following equation,

$$\frac{C_e}{q_e} = \frac{1}{q_m K_a} + \frac{C_e}{q_m} \tag{6}$$

Table 1
Intra-particle diffusion for the adsorption of Cr(VI) onto composite nanofibers.

| C$_0$ (mg/L)	q$_{e, exp}$ (mg/g)	Nonlinear Pseudo-first-order model			Nonlinear Pseudo-second-order model			Intra-particle diffusion model		
		k$_1$ (1/min)	q$_{e,cal}$ (mg/g)	R^2	k$_1$ (1/min)	q$_{e,cal}$ (mg/g)	R^2	K$_{id}$ (mg/g/min$^{1/2}$)	C	R^2
10	24.9	0.092	25.03	0.998	0.0062	26.67	0.959	4.54	0.155	0.994
20	49.85	0.071	50.09	0.998	0.0022	53.88	0.958	7.94	0.067	0.987
30	74.75	0.057	72.39	0.995	0.0011	78.95	0.981	9.81	1.76	0.969
50	124.625	0.0388	124.14	0.996	3.83E−4	137.30	0.973	16.28	−7.47	0.9888
80	199.575	0.0338	193.85	0.986	2.01E−4	217.47	0.969	26.13	−20.55	0.951
100	249.5	0.0285	243.97	0.998	1.28E−4	276.47	0.974	30.13	−25.71	0.937
200	490.75	0.0216	487.70	0.983	4.72E−5	550.87	0.962	35.45	−35.55	0.897
300	704.125	0.0164	714.27	0.987	1.95E−5	861.11	0.969	53.46	−54.65	0.89

Fig. 5. Intra-particle diffusion plot of Cr(VI) adsorption, pH = 2, and T = 20 °C.

Table 2
Langmuir, Freundlich, Redlich-Peterson and Temkin Isotherm constants parameters for the adsorption of Cr(VI) onto the composite nanofibers.

Model	Parameters	Linear Temperature (°C)			Nonlinear Temperature (°C)		
		20	40	60	20	40	60
Langmuir	$q_{Max.}$ (mg/g)	500	516	527	732	704.7	584.8
	K_L (L/mg)	0.002	0.002	0.002	0.02	0.028	0.074
	R^2	0.861	0.913	0.963	0.963	0.932	0.863
Freundlich	n	3.77	4.32	4.62	1.89	2.3	3.46
	K_F (mg g)	0.53	0.41	0.37	43.2	70.3	138.3
	R^2	0.988	0.986	0.996	0.986	0.979	0.908
Redlich-Peterson	g	0.828	0.952	0.968	0.47	0.57	0.71
	K_R (L mg$^{1-1/A}$)	86.52	296.33	530.32	4.57E6	5.03E6	9.54E6
	α_R	1.05	4.15	7.62	1.97E8	3.54E8	1.32E9
	R^2	0.980	0.984	0.984	0.984	0.975	0.889
Temkin	A_T (L/g)	119.3	183.54	256.95	–	–	–
	b_T (kJ/mol)	47.78	33.53	30.75	–	–	–
	R^2	0.632	0.581	0.635	–	–	–
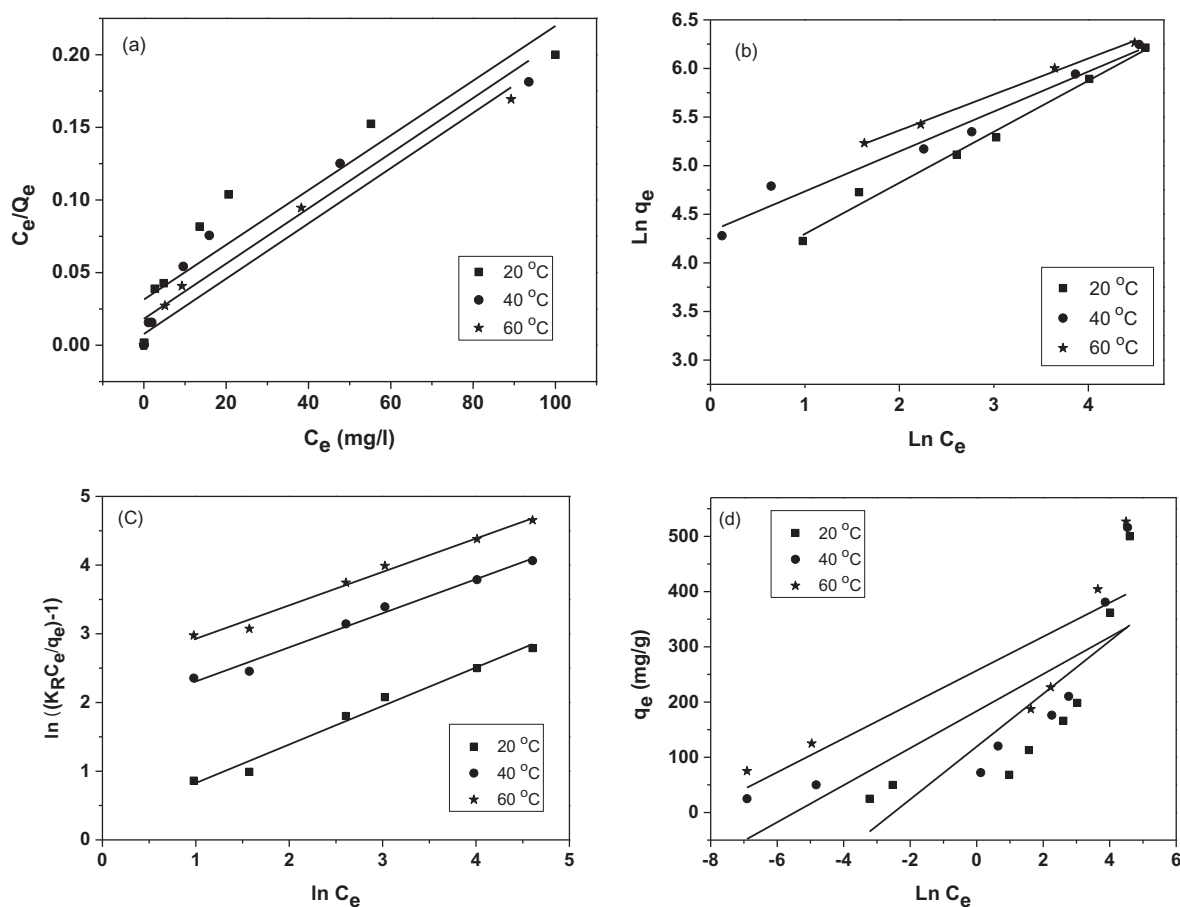
Fig. 6. (a) Linear Langmuir isotherm model, (b) Freundlich isotherm model, (c) Redlich-Peterson isotherm model, and (d) Temkin isotherm model for adsorption of Cr(VI) using PAN-CNT/TiO$_2$-NH$_2$ nanofibers at different temperature (pH = 2).

$$q_e = \frac{q_m K_a C_e}{1 + K_a C_e} \tag{7}$$

The Freundlich model is used to describe reversible adsorption and the adsorption onto a heterogeneous surface, which is expressed as follows:

$$\log q_e = \log K_F + \frac{1}{n} \log C_e \tag{8}$$

$$q_e = K_F C_e^{1/n} \tag{9}$$

The Redlich-Peterson isotherm contains three parameters, K_R, α_R and g, incorporates the features of the Langmuir and the Freundlich isotherms [55]. It may be used to represent adsorption equilibrium over a wide concentration range of adsorbate. The exponent, g, lies between 0 and 1. When g = 1, the Redlich–Peterson equation becomes the Langmuir equation, and when g = 0, it becomes the Henry's law. This isotherm is described as follows:

$$\ln \left(K_R \frac{C_e}{q_e} - 1 \right) = g \ln(C_e) + \ln(\alpha_R) \tag{10}$$

$$q_e = \frac{K_R C_e}{1 + \alpha_R C_e^g} \tag{11}$$

Furthermore, Temkin isotherm model is used to evaluate the sorption potential of the sorbent for Cr(VI), and assumes that the fall in the heat of sorption is linear rather than logarithmic, as implied in the Freundlich equation [56]. The Temkin isotherm has generally been applied in the following form [57]:

$$q_e = \frac{RT}{b_T} \ln(A_T C_e) \tag{12}$$

where q_e is the amount adsorbed at equilibrium (mg/g), C_e is the equilibrium concentration of the solution (mg/L), q_m is the maximum adsorption capacity (mg/g), k_a is a Langmuir constant related to the affinity of the binding sites and energy of adsorption (L/g), k_F is a Freundlich constant $(mg/g)(L/mg)^{1/n}$, which related to the adsorption capacity, $1/n$ is the heterogeneity factor representing the deviation from linearity of adsorption and is also known as Freundlich coefficient, K_R, α_R, and g ($0 < g < 1$), are three isotherm constants, A_T is the equilibrium binding constant corresponding to the maximum binding energy (L/g), b_T is the Temkin constant related to the heat of adsorption (kJ/mol), R is the universal gas constant (8.314 J/mol/K) and T is the absolute temperature (K). The values of the maximum loading capacity of Cr(VI) for linear and nonlinear Langmuir, Freundlich, Redlich-Peterson, and Temkin models can be are presented as shown in Figs. 6–8 and the obtained kinetic parameters are summarized in Table 2. The results indicate that the

adsorption capacity increase as the temperature increases which confirms that the adsorption process is endothermic [50]. This may be due to an increase in thermal energy of the adsorbing species, which leads to higher adsorption capacity and faster adsorption rate. The very high values of correlation coefficients (R^2) indicate that the Freundlich model fitted well the isotherm data better than the Langmuir, Redlich-Peterson and Temkin models and confirms the multilayer adsorption of Cr(VI) onto the composite surface.

3.5. Thermodynamic study

To evaluate the influence of temperature on the adsorption process of Cr(VI) onto the composite nanofibers, the thermodynamic parameters such as Gibbs free energy (ΔG^0), enthalpy (ΔH^0), and entropy (ΔS^0) are calculated using the following equations [58]:

$$\ln K_d = \frac{\Delta S^0}{R} + \frac{-\Delta H^0}{RT} \tag{13}$$

$$K_d = \frac{(C_0 - C_e)V}{mC_e} \tag{14}$$

$$\Delta G^0 = \Delta H^0 - T\Delta S^0 \tag{15}$$

where R is the universal gas constant (8.314 J/mol K), T is the absolute temperature (K), m is the adsorbent dose (g), and K_d is the thermodynamic equilibrium constant (L/mol). The values of ΔH^0 and
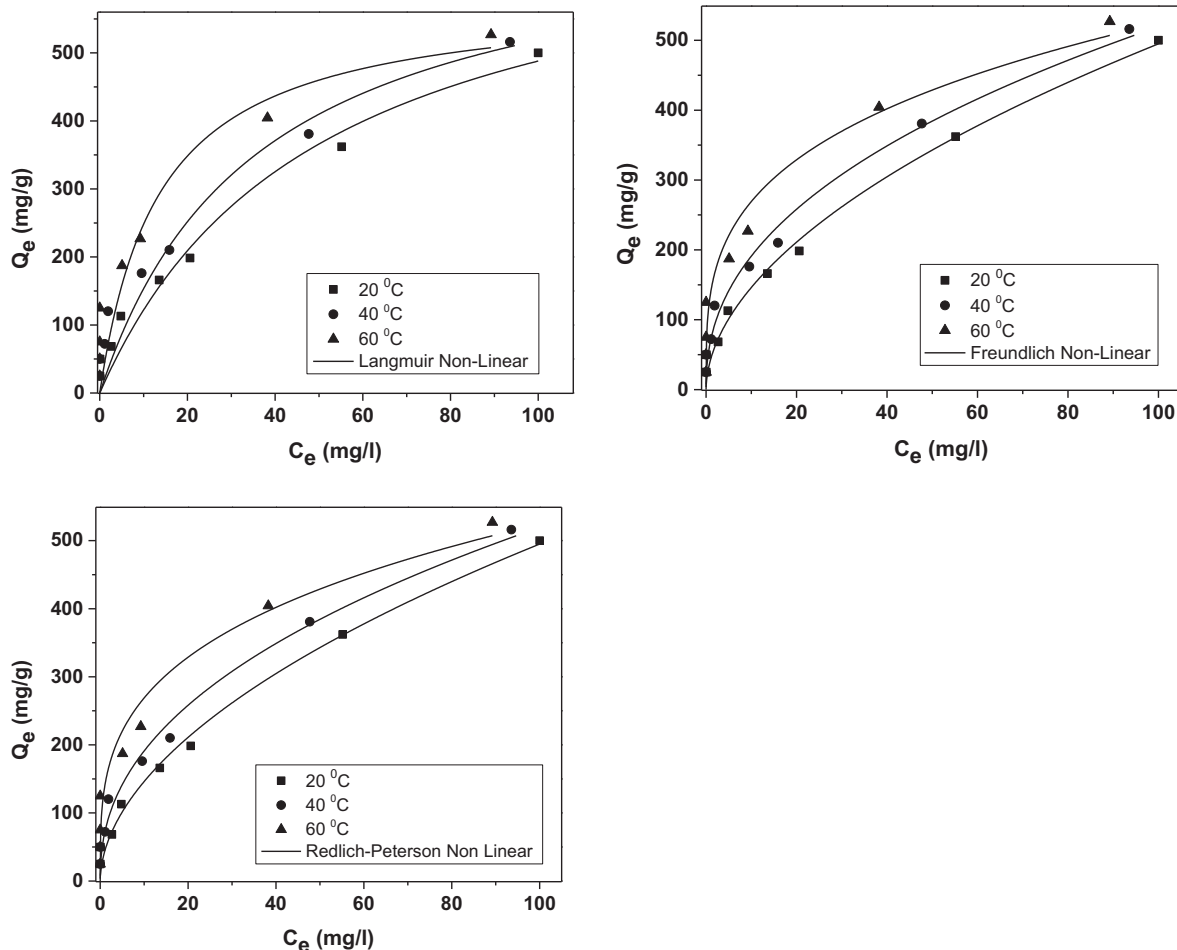

Fig. 7. Nonlinear Langmuir isotherm model, Freundlich isotherm model, Redlich-Peterson isotherm model for adsorption of Cr(VI) using composite nanofibers at different temperature (pH = 2).
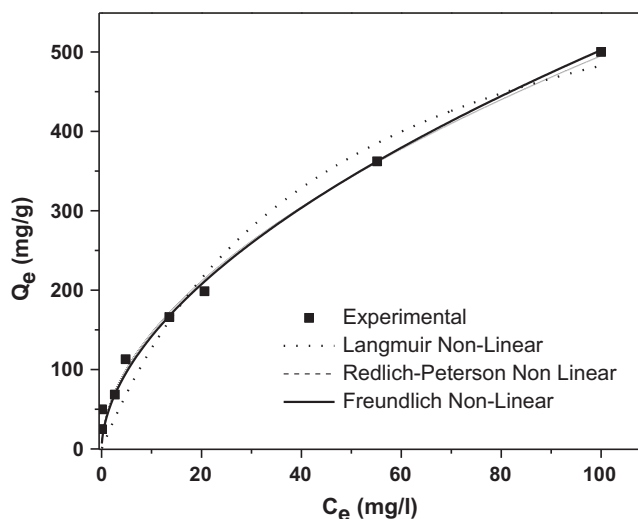
Fig. 8. Nonlinear Langmuir isotherm model, Freundlich isotherm model, Redlich-Peterson isotherm model for adsorption of Cr(VI) using composite nanofibers (pH = 2, 20 °C).
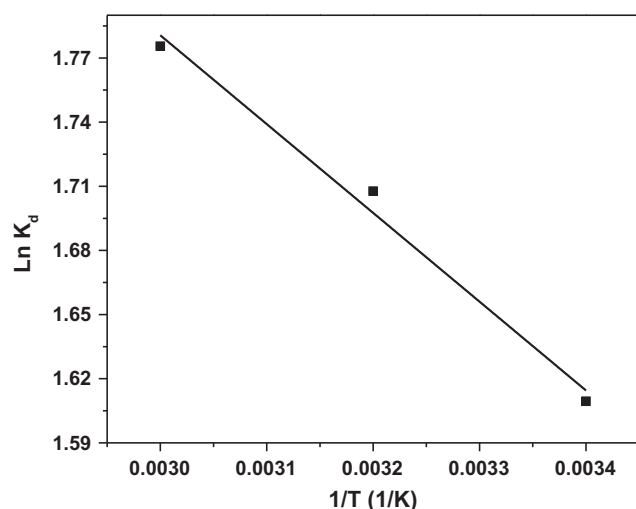

Fig. 9. Thermodynamic parameters of Cr(VI) adsorption onto composite nanofibers.

ΔS^0 were obtained from the slope and intercept of the plot of ln K_d versus 1/T as shown in Fig. 9 and Table 3. The negative value of energy ΔG^0 suggests that the adsorption process is feasible and spontaneous. In general, the values of energy ΔG^0 in between 0 and −20 kJ/mol indicate that the adsorption process is physisorption, while the values in between −80 and −4000 kJ/mol correspond to chemisorptions [59,60]. In experimental results, the values of energy ΔG^0 suggest that the adsorption is a chemisorption process. As the value of ΔH^0 is negative, we can infer that the adsorption reaction is exothermic. This implies that the adsorption

Table 3
Thermodynamic parameters for Cr(VI) adsorbed by PAN-CNT/TiO$_2$-NH$_2$ composite nanofibers.

T (K)	ΔG^0 (kJ/mol)	ΔS^0 (kJ/(K/mol))	ΔH^0 (kJ/mol)
293	−1301.89	3.026	−415.21
313	−1362.42		
333	−1422.94		

process is energetically stable. The positive value of ΔS^0 reflects the increased disorder and randomness of the Cr(VI) on the composite nanofibers at the solid/liquid solution interface during the adsorption process, and indicate the affinity of the adsorbent material toward Cr(VI) [61].

3.6. Adsorption mechanism

In order to confirm the adsorption mechanism, UV–vis and XPS were used, and the results are shown in Fig. 10. Fig. 10a shows that the maximum absorption wavelength of Cr(VI) is 351 nm with an absorbance of 0.94 before adsorption, and after adsorption the absorbance decreased, indicating complete removal of Cr(VI) ions. Further to confirm the reduction process involved in the removal of Cr(VI), the composite nanofibers after adsorption were analyzed with XPS. The XPS results in Fig. 10b shows that after the adsorption process, two energy bands at about 579.2 and 588.3 eV appeared, which correspond to the binding energies of Cr 2p$_{3/2}$ and Cr 2p$_{1/2}$ orbitals, respectively which are consistent with Cr (III) and Cr(VI) [62]. The existence of the Cr(VI) on the nanofibers is attributable to the anion exchange between doped Cl$^-$ in the adsorbent and Cr(VI) ions in the aqueous solution [63]. The presence of Cr(III) (binding energy of 577.1 and 586.5 eV) on the nanofibers surface suggests that some fraction of adsorbed Cr(VI) was reduced to Cr(III) by a reduction process [50]. This behavior attributable to the reduction of the Cr(VI) by the TiO$_2$, which indicates that TiO$_2$ has a strong reduction capability for Cr(VI) [28,64]. Overall, Cr(VI) is removed either by adsorbed on the surface of composite nanofibers or by being reduced into Cr(III), which is much less toxic. To sum up, the interaction of Cr with the composite nanofibers includes two process, adsorption (including both Cr(VI) and Cr (III) species) and reduction [65].

3.7. Effect of adsorbent dosage

The effect of the amount of sorbent dose as a function of time on the adsorption performance of Cr(VI) was studied by varying the amount of the TiO$_2$ NPs ranging from 5 to 40 mg as shown in Fig. 11. The result indicated that the adsorption performance increases from 55.2% to 99.7% with an increase in adsorbent dose. This is attributed to the fact that as the mass of sorbent is increased, the total number of active sites on the sorbent surface also increases thereby resulting in an increase in a number of electrons which can be used for the removal of Cr(VI) [66]. With increasing the amount of TiO$_2$ NPs dose above 30 mg on the surface of nanofibers, the dosage was aggregation. Therefore, reduces the penetration of light and the adsorption reaches a saturation level at high doses. This behavior can be attributed due to when the concentration of the sorbent exceeds an optimum value, the adsorption performance may decrease due to a decrease in the number of active sites on the TiO$_2$ NPs surface available for Cr(VI) removal thereby resulting into a decrease in the performance of the adsorption [67].

3.8. Regeneration and reusability studies

Regeneration and reuse of the adsorbent material are an important factors in wastewater treatment processes for evaluating the cost effectiveness. The composite nanofibers were washed with 0.1 M NaOH to check the regeneration and reusability of PAN-CNT/TiO$_2$-NH$_2$ nanofiber for Cr(VI) removal. The Cr(VI) adsorption capacity still remained by 80% after 5 times usage. However, the removal percentage was declined gradually after five adsorption-desorption cycles, which may be attributed to the deformation of nanofibers in NaOH medium during regeneration. These results indicate that the PAN-CNT/TiO$_2$-NH$_2$ nanofiber could be regener-
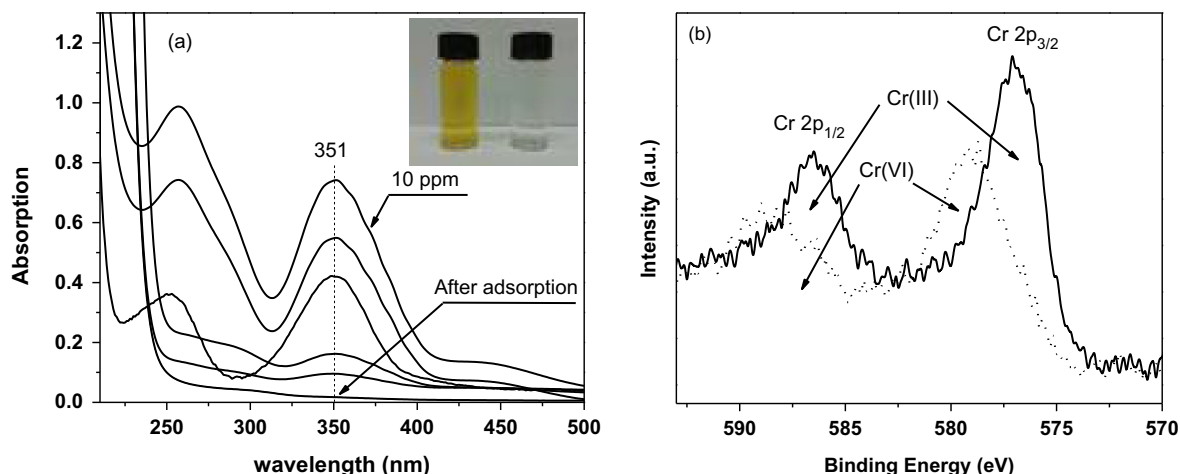
Fig. 10. (a) UV–vis spectra, and (b) XPS of Cr(VI) solution before and after adsorption (Cr(VI) = 10 ppm, pH = 2, and T = 20 °C).
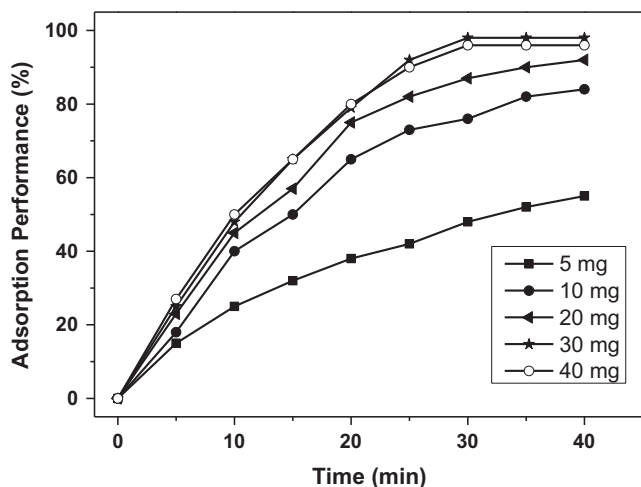

Fig. 11. Effect of TiO$_2$ NPs sorbent dose on the adsorption performance of Cr (VI) using PAN-CNT/TiO$_2$-NH$_2$ composite nanofibers. (Cr (VI) = 10 ppm, pH = 2, 40 min).

ated upon NaOH treatment and may be reused for further Cr(VI) removal up to five cycles.

4. Conclusions

The as-prepared PAN-CNT/TiO$_2$-NH$_2$ composite nanofibers were successfully prepared by the electrospinning technique and can be used as an adsorbent. The composite nanofibers showed an excellent ability to remove Cr(VI) ions in water, especially in the acidic environment. The introduction of NH$_2$ groups to the TiO$_2$ surface can significantly increase the adsorption capacity of the composite nanofibers for heavy metal removal. The highest adsorption capacity of PAN-CNT/TiO$_2$-NH$_2$ for Cr (VI) is found to be 714.27 mg/g at 293 K, and the process can be better described using the nonlinear pseudo first order model than the pseudo second order model. Isotherm data fitted well to the Freundlich isotherm model and the maximum adsorption capacity increased with the increase in temperature. It is found in this study that the Cr (VI) adsorption processes has reached their equilibrium state in about 30 min, which is faster than most of TiO$_2$ adsorbents used before. The negative value of ΔH°Confirms that the adsorption process is exothermic. UV–vis and XPS were the main mechanism for the Cr(VI) adsorption. Desorption results show that the adsorption capacity can remain up to 80% after 5 usage cycles. This research demon-

strates that PAN-CNT/TiO$_2$-NH$_2$ can be an effective adsorbent for toxic heavy metal removal.

References

[1] L. Khezami, Richard Capart, Removal of chromium(VI) from aqueous solution by activated carbons: kinetic and equilibrium studies, J. Hazard. Mater. 123 (1–3) (2005) 223–231.

[2] X. Guo, Guang Tao Fei, Hao Su, Li De Zhang, High-performance and reproducible polyaniline nanowire/tubes for removal of Cr(VI) in aqueous solution, J. Phys. Chem. C 115 (5) (2011) 1608–1613.

[3] J.A. Giménez, M.A. Aguado, S. Cervera-March, Photocatalytic reduction of chromium(VI) with titania powders in a flow system. Kinetics and catalyst activity. J. Mol. Catal. A: Chem. 105(1) (1996) 67–78.

[4] Y. Ku, In-Liang Jung, Photocatalytic reduction of Cr(VI) in aqueous solutions by UV irradiation with the presence of titanium dioxide, Water Res. 35 (1) (2001) 135–142.

[5] L.B.M. Khalil, W.E. Mourad, M.W. Rophael, Photocatalytic reduction of environmental pollutant Cr(VI) over some semiconductors under UV/visible light illumination, Appl. Catal. B: Environ. 17(3) (1998) 267–273.

[6] J.-H. Zhu, Xi-Luan Yan, Ye Liu, Bao Zhang, Improving alachlor biodegradability by ferrate oxidation, J. Hazard. Mater. 135 (1–3) (2006) 94–99.

[7] Y.C. Sharma, Effect of temperature on interfacial adsorption of Cr(VI) on wollastonite, J. Colloid Interf. Sci. 233 (2) (2001) 265–270.

[8] K. Chon et al., Combined coagulation-disk filtration process as a pretreatment of ultrafiltration and reverse osmosis membrane for wastewater reclamation: an autopsy study of a pilot plant, Water Res. 46 (6) (2012) 1803–1816.

[9] J. Doménech, Javier Muñoz, Photocatalytical reduction of Cr(VI) over ZnO powder, Electrochim. Acta 32 (9) (1987) 1383–1386.

[10] C.-J. Cheng, Tzu-Huei Lin, Chiou-Pin Chen, Kai-Wei Juang, Dar-Yuan Lee, The effectiveness of ferrous iron and sodium dithionite for decreasing resin-extractable Cr(VI) in Cr(VI)-spiked alkaline soils, J. Hazard. Mater. 164 (2–3) (2009) 510–516.

[11] D. Akretche, G.D., M. Taleb Ahmed, R. Maachi, S. Taha, T. Chaabane, Nanofiltration process applied to the tannery solutions, Desalination 200 (2006) 419–420.

[12] C.K.P. Ahn, Donghee Park, Seung H. Woo, Jong M. Park, Removal of cationic heavy metal from aqueous solution by activated carbon impregnated with anionic surfactants, J. Hazard. Mater. 164(2–3) (2009) 1130–1136.

[13] R.M.C. Schneider, C.F. Cavalin, M.A.S.D. Barros, C.R.G. Tavares, Adsorption of chromium ions in activated carbon, Chem. Eng. J. 132(1–3) (2007) 355–362.

[14] Z. Hu, Lin Lei, Yijiu Li, Yaming Ni, Chromium adsorption on high-performance activated carbons from aqueous solution, Sep. Purif. Technol. 31 (1) (2003) 13–18.

[15] T. Burks, A. Uheida, M. Saleemi, M. Eita, M.S. Toprak, M. Muhammed, Removal of chromium(VI) using surface modified superparamagnetic iron oxide nanoparticles, Separat. Sci. Technol. 48(8) (2013) 1243–1251.

[16] D. Lu, Gaoke Zhang, Zhen Wan, Visible-light-driven g-C3N4/Ti3+-TiO2 photocatalyst co-exposed {0 0 1} and {1 0 1} facets and its enhanced photocatalytic activities for organic pollutant degradation and Cr(VI) reduction, Appl. Surf. Sci. 358 (Part A) (2015) 223–230.

[17] A.B. Albadarin, Chirangano Mangwandi, Gavin M. Walker, Stephen J. Allen, Mohammad N.M. Ahmad, Majeda Khraisheh, Influence of solution chemistry on Cr(VI) reduction and complexation onto date-pits/tea-waste biomaterials, J. Environ. Manage. 114 (2013) 190–201.

[18] Y. Hou, Huijuan Liu, Xu Zhao, Jiuhui Qu, J.P. Chen, Combination of electroreduction with biosorption for enhancement for removal of hexavalent chromium, J. Colloid Interf. Sci. 385 (1) (2012) 147–153.

[19] Alaa Mohamed, T.A. Osman, M.S. Toprak, M. Muhammed, A. Uheida, Surface functionalized composite nanofibers for efficient removal of arsenic from aqueous solutions, Chemosphere 180 (2017) 108–116.

[20] Alaa Mohamed, S. Yousef, M.A. Abdelnaby, T.A. Osman, M.S. Toprak, M. Muhammed, B. Hamawandi, A. Uheida, Photocatalytic degradation of organic dyes and enhanced mechanical properties of PAN/CNTs composite nanofibers, Sep. Purif. Technol. 182 (2017) 219–223.

[21] Waleed Khalil, A. Mohamed, Mohamed Bayoumi, T.A. Osman, Tribological properties of dispersed carbon nanotubes in lubricant, Fullerenes, Nanotubes, Carbon Nanostruct. 24 (7) (2016) 479–485.

[22] Bahaa M. Kamel, A. Mohamed, M. El Sherbiny, K.A. Abed, Tribological behaviour of calcium grease containing carbon nanotubes additives, Ind. Lubr. Tribol. 68 (6) (2016) 723–728.

[23] Alaa Mohamed, T.A. Osman, Ali Khattab, M. Zaki, Tribological behavior of carbon nanotubes as an additive on lithium grease, J. Tribol. 137 (1) (2014) 011801.

[24] Samy Yousef, Alaa Mohamed, Mass production of CNTs using CVD multi-quartz tubes, J. Mech. Sci. Technol. 30 (11) (2016) 5135–5141.

[25] Bahaa M. Kamel, A. Mohamed, M. El Sherbiny, K.A. Abed, M. Abd-Rabou, Rheological characteristics of modified calcium grease with graphene nanosheets, Fullerenes, Nanotubes, Carbon Nanostruct. 25 (6) (2017).

[26] Bahaa M. Kamel, A. Mohamed, M. El Sherbiny, K.A. Abed, M. Abd-Rabou, Tribological properties of graphene nanosheets as an additive in calcium grease, J. Dispersion Sci. Technol. 38 (10) (2016) 1495–1500.

[27] Alaa Mohamed, T.A. Osman, M.S. Toprak, M. Muhammed, Ramy El-Sayed, A. Uheida, Composite nanofibers for highly efficient photocatalytic degradation of organic dyes from contaminated water, Environ. Res. 145 (2016) 18–25.

[28] Alaa Mohamed, T.A. Osman, M.S. Toprak, M. Muhammed, Eda Yilmaz, A. Uheida, Visible light photocatalytic reduction of Cr(VI) by surface modified CNT/titanium dioxide composites nanofibers, J. Mol. Catal. A: Chem. 424 (2016) 45–53.

[29] M. Avila, T. Burks, F. Akhtar, M. Göthelid, P.C. Lansåker, M.S. Toprak, M. Muhammed, A. Uheida, Surface functionalized nanofibers for the removal of chromium(VI) from aqueous solutions, Chem. Eng. J. 245 (2014) 201–209.

[30] S. Xing, Dongyuan Zhao, Wenjuan Yang, Zichuan Ma, Wu Yinsu, Yuanzhe Gao, Weirong Chen, Jiao Han, Fabrication of magnetic core-shell nanocomposites with superior performance for water treatment, J. Mater. Chem. A 1 (5) (2013) 1694–1700.

[31] N. Talreja, Dinesh Kumar, Nishith Verma, Removal of hexavalent chromium from water using Fe-grown carbon nanofibers containing porous carbon microbeads, J. Water Process Eng. 3 (2014) 34–45.

[32] J. Chen, Xiaoqin Hong, Qingdong Xie, Diankai Li, Qianfeng Zhang, Highly efficient removal of chromium(VI) from aqueous solution using polyaniline/sepiolite nanofibers, Water Sci. Technol. 70 (7) (2014) 1236.

[33] J. Wang, Kai Pan, Emmanuel P. Giannelis, Bing Cao, Polyacrylonitrile/polyaniline core/shell nanofiber mat for removal of hexavalent chromium from aqueous solution: mechanism and applications, RSC Adv. 3 (23) (2013) 8978–8987.

[34] F. Liu, Xinhong Wang, Bor-Yann Chen, Shilin Zhou, Chang-Tang Chang, Removal of Cr(VI) using polyacrylonitrile/ferrous chloride composite nanofibers, J. Taiwan Inst. Chem. Eng. 70 (2017) 401–410.

[35] Alaa Mohamed, T.A. Osman, Ali Khattab, M. Zaki, Rheological behavior of carbon nanotubes as an additive on lithium grease, J. Nanotechnol. 2013 (2013) 4.

[36] Bahaa M. Kamel, A. Mohamed, M. El Sherbiny, K.A. Abed, Rheology and thermal conductivity of calcium grease containing multi-walled carbon nanotube, Fullerenes, Nanotubes, Carbon Nanostruct. 24 (4) (2016) 260–265.

[37] M.-C. Lu, Gwo-Dong Roam, Jong-Nan Chen, C.P. Huang, Factors affecting the photocatalytic degradation of dichlorvos over titanium dioxide supported on glass, J. Photochem. Photobiol., A 76 (1) (1993) 103–110.

[38] F. Zheng, Zhenhua Wang, Jie Chen, ShunXing Li, Synthesis of carbon quantum dot-surface modified P25 nanocomposites for photocatalytic degradation of p-nitrophenol and acid violet 43, RSC Adv. 4 (58) (2014) 30605–30609.

[39] Z. Wan, Gaoke Zhang, Xiaoyong Wu, Shu Yin, Novel visible-light-driven Z-scheme Bi12GeO20/g-C3N4 photocatalyst: oxygen-induced pathway of organic pollutants degradation and proton assisted electron transfer mechanism of Cr(VI) reduction, Appl. Catal. B 207 (2017) 17–26.

[40] N.A. Oladoja, I.A. Ololade, V.O. Olatujoye, T.A. Akinnifesi, Performance evaluation of fixed bed of nano calcium oxide synthesized from a gastropod shell (Achatina achatina) in hexavalent chromium abstraction from aqua system, Water, Air, Soil Pollut. 223 (4) (2012) 1861–1876.

[41] R. Liang, Lijuan Shen, Fenfen Jing, Weiming Wu, Na Qin, Rui Lin, Ling Wu, NH2-mediated indium metal–organic framework as a novel visible-light-driven photocatalyst for reduction of the aqueous Cr(VI), Appl. Catal. B 162 (2015) 245–251.

[42] D. Chauhan, J. Dwivedi, N. Sankararamakrishnan, Novel chitosan/PVA/zerovalent iron biopolymeric nanofibers with enhanced arsenic removal applications, Environ. Sci. Pollut. Res. 21 (15) (2014) 9430–9442.

[43] L.-L. Min et al., Preparation of chitosan based electrospun nanofiber membrane and its adsorptive removal of arsenate from aqueous solution, Chem. Eng. J. 267 (2015) 132–141.

[44] N. Mahanta, S. Valiyaveettil, Functionalized poly(vinyl alcohol) based nanofibers for the removal of arsenic from water, RSC Adv. 3 (8) (2013) 2776–2783.

[45] D. Morillo et al., Arsenate removal with 3-mercaptopropanoic acid-coated superparamagnetic iron oxide nanoparticles, J. Colloid Interf. Sci. 438 (2015) 227–234.

[46] M. Bhaumik et al., Polyaniline/Fe0 composite nanofibers: an excellent adsorbent for the removal of arsenic from aqueous solutions, Chem. Eng. J. 271 (2015) 135–146.

[47] W.J. Weber, J.C. Morris, Kinetics of adsorption carbon from solutions, J. Sanit. Eng. Div. Proc. Am. Soc. Civ. Eng. 89 (1963) 31–60.

[48] K. Gupta, Uday Chand Ghosh, Arsenic removal using hydrous nanostructure iron(III)–titanium(IV) binary mixed oxide from aqueous solution, J. Hazard. Mater. 161 (2–3) (2009) 884–892.

[49] B.H. Hameed, Equilibrium and kinetic studies of methyl violet sorption by agricultural waste, J. Hazard. Mater. 154 (1–3) (2008) 204–212.

[50] M. Bhaumik, Arjun Maity, V.V. Srinivasu, Maurice S. Onyango, Removal of hexavalent chromium from aqueous solution using polypyrrole-polyaniline nanofibers, Chem. Eng. J. 181–182 (2012) 323–333.

[51] K.Y. Foo, B.H. Hameed, Insights into the modeling of adsorption isotherm systems, Chem. Eng. J. 156 (1) (2010) 2–10.

[52] L. Zhang et al., Isotherm study of phosphorus uptake from aqueous solution using aluminum oxide, CLEAN – Soil, Air Water 38 (9) (2010) 831–836.

[53] M. Brdar et al., Comparison of two and three parameters adsorption isotherm for Cr(VI) onto Kraft lignin, Chem. Eng. J. 183 (2012) 108–111.

[54] K.-Y.H. Shin, Jin-Yong Hong, Jyongsik Jang, Heavy metal ion adsorption behavior in nitrogen-doped magnetic carbon nanoparticles: Isotherms and kinetic study, J. Hazard. Mater. 190 (1–3) (2011) 36–44.

[55] P. Gogoi, Dutta Debasish, T.K. Maji, Equilibrium and kinetics study on removal of arsenate ions from aqueous solution by CTAB/TiO2 and starch/CTAB/TiO2 nanoparticles: a comparative study, J. Water Health (5) (2016).

[56] C. Aharoni, Moshe Ungarish, Kinetics of activated chemisorption. Part 2. – Theoretical models, J. Chem. Soc., Faraday Trans. 1: Phys. Chem. Condens. Phases 73 (1977) 456–464.

[57] Y.S.P. Ho, J.F. Porter, G. McKay, Equilibrium isotherm studies for the sorption of divalent metal ions onto peat: copper, nickel and lead single component systems, Water, Air, Soil Pollut. 141 (1) (2002) 1–33.

[58] T. Ren, Ping He, Weiling Niu, Yanjun Wu, Lunhong Ai, Xinglong Gou, Synthesis of α-Fe2O3 nanofibers for applications in removal and recovery of Cr(VI) from wastewater, Environ. Sci. Pollut. Res. 20 (1) (2013) 155–162.

[59] A.N. Fernandes, Carlos Alberto Policiano Almeida, Nito Angelo Debacher, Maria Marta de Souza Sierra, Isotherm and thermodynamic data of adsorption of methylene blue from aqueous solution onto peat, J. Mol. Struct. 982 (1–3) (2010) 62–65.

[60] C.-H. Weng, Yao-Tung Lin, Tai-Wei Tzeng, Removal of methylene blue from aqueous solution by adsorption onto pineapple leaf powder, J. Hazard. Mater. 170 (1) (2009) 417–424.

[61] N.H. Nasuha, B.H. Hameed, Adsorption of methylene blue from aqueous solution onto NaOH-modified rejected tea, Chem. Eng. J. 166 (2) (2011) 783–786.

[62] J. Hu, Guohua Chen, Irene M.C. Lo, Removal and recovery of Cr(VI) from wastewater by maghemite nanoparticles, Water Res. 39 (18) (2005) 4528–4536.

[63] M. Bhaumik, Arjun Maity, V.V. Srinivasu, Maurice S. Onyango, Enhanced removal of Cr(VI) from aqueous solution using polypyrrole/Fe3O4 magnetic nanocomposite, J. Hazard. Mater. 190 (1–3) (2011) 381–390.

[64] J. Wang, Kai Pan, Qiwei He, Bing Cao, Polyacrylonitrile/polypyrrole core/shell nanofiber mat for the removal of hexavalent chromium from aqueous solution, J. Hazard. Mater. 244–245 (2013) 121–129.

[65] C.-J. Li, Shan-Shan Zhang, Jiao-Na Wang, Ting-Yue Liu, Preparation of polyamides 6 (PA6)/Chitosan@FexOy composite nanofibers by electrospinning and pyrolysis and their Cr(VI)-removal performance, Catal. Today 224 (2014) 94–103.

[66] H. Fida, Sheng Guo, Gaoke Zhang, Preparation and characterization of bifunctional Ti–Fe kaolinite composite for Cr(VI) removal, J. Colloid Interf. Sci. 442 (2015) 30–38.

[67] X. Meng, Gaoke Zhang, Neng Li, Bi24Ga2O39 for visible light photocatalytic reduction of Cr(VI): controlled synthesis, facet-dependent activity and DFT study, Chem. Eng. J. 314 (2017) 249–256.